






Article

Putting a “C₆₀ Ball” and Chain to Chlorin e6 Improves Its Cellular Uptake and Photodynamic Performances

Manuele Di Sante^{1,†}, Alena Kaltenbrunner^{2,†}, Marco Lombardo¹, Alberto Danielli²,
Paolo Emidio Costantini^{2,*}, Matteo Di Giosia^{1,*} and Matteo Calvaresi^{1,*}

¹ Dipartimento di Chimica “Giacomo Ciamician”, Alma Mater Studiorum—Università di Bologna, Via Francesco Selmi 2, 40126 Bologna, Italy; manuele.disante2@unibo.it (M.D.S.); marco.lombardo@unibo.it (M.L.)

² Dipartimento di Farmacia e Biotecnologie, Alma Mater Studiorum—Università di Bologna, Via Francesco Selmi 3, 40126 Bologna, Italy; alena.kaltenbrunner2@unibo.it (A.K.); alberto.danielli@unibo.it (A.D.)

* Correspondence: paolo.costantini4@unibo.it (P.E.C.); matteo.digiosia2@unibo.it (M.D.G.); matteo.calvaresi3@unibo.it (M.C.)

† These authors contributed equally to this work.

Abstract: Chlorin e6 (Ce6) and fullerene (C₆₀) are among the most used photosensitizers (PSs) for photodynamic therapy (PDT). Through the combination of the chemical and photophysical properties of Ce6 and C₆₀, in principle, we can obtain an “ideal” photosensitizer that is able to bypass the limitations of the two molecules alone, i.e., the low cellular uptake of Ce6 and the scarce solubility and absorption in the red region of the C₆₀. Here, we synthesized and characterized a Ce6–C₆₀ dyad. The UV-Vis spectrum of the dyad showed the typical absorption bands of both fullerene and Ce6, while a quenching of Ce6 fluorescence was observed. This behavior is typical in the formation of a fullerene–antenna system and is due to the intramolecular energy, or electron transfer from the antenna (Ce6) to the fullerene. Consequently, the Ce6–C₆₀ dyad showed an enhancement in the generation of reactive oxygen species (ROS). Flow cytometry measurements demonstrated how the uptake of the Ce6 was strongly improved by the conjugation with C₆₀. The Ce6–C₆₀ dyad exhibited in A431 cancer cells low dark toxicity and a higher PDT efficacy than Ce6 alone, due to the enhancement of the uptake and the improvement of ROS generation.

Keywords: Chlorin e6 (Ce6); C₆₀; photodynamic therapy (PDT); antenna system; phototheranostics



Citation: Di Sante, M.; Kaltenbrunner, A.; Lombardo, M.; Danielli, A.; Costantini, P.E.; Di Giosia, M.; Calvaresi, M. Putting a “C₆₀ Ball” and Chain to Chlorin e6 Improves Its Cellular Uptake and Photodynamic Performances. *Pharmaceuticals* **2023**, *16*, 1329. <https://doi.org/10.3390/ph16091329>

Academic Editor: Veronika Huntosova

Received: 28 July 2023

Revised: 8 September 2023

Accepted: 11 September 2023

Published: 20 September 2023



Copyright: © 2023 by the authors. Licensee MDPI, Basel, Switzerland. This article is an open access article distributed under the terms and conditions of the Creative Commons Attribution (CC BY) license (<https://creativecommons.org/licenses/by/4.0/>).

1. Introduction

An ideal photosensitizer [1,2] must have both photophysical and drug-like properties, including: (i) a high quantum yield of the intersystem crossing process, (ii) the generation of ROS with both type I and type II mechanisms, (iii) intense absorption in the “tissue optical window” (from 650 to 1350 nm), (iv) resistance to photodegradation, (v) accumulation in cancer cells, (vi) negligible dark toxicity, and (vii) high solubility and stability in physiological environments.

Chlorin e6 (Ce6) [3–5] and fullerene (C₆₀) [6–15] are among the most known photosensitizers (PSs) for photodynamic therapy (PDT). On one side, Ce6 possesses a significant absorption in the red region of the visible spectrum and an intense fluorescence that may be used to develop theranostic applications [3–5]. However, due to its negative charges, Ce6 shows a poor cellular uptake, which determines a low accumulation in cancer cells [3–5]. The penetration of a photosensitizer into the cell is a crucial step to perform an efficient PDT treatment. To bypass this drawback, many Ce6 derivatives [3–5,16–20] and ad hoc delivery systems [3–5,21–27] were developed, aiming to improve Ce6 accumulation in cancer cells through passive and active targeting.

On the other side, fullerene C_{60} follows both the photophysical mechanisms (type I and II mechanisms) involved in the production of ROS, is highly resistant to photobleaching [6–9], and exhibits a strong tendency to pass the cellular membrane (it is commonly used as a delivery system [28–30]). However, the extremely low solubility of C_{60} , even in organic solvents, and its poor absorption in the visible region of the spectrum limit its application in PDT [6–9]. Chemical functionalization of the fullerene cage can improve its solubility, while the use of “antenna systems” can enhance its photodynamic activity in the visible region [31–38]. The molecular antenna (donor) acts as a light collector, absorbing the light in the desired visible spectral region and then transferring the excitation energy or electrons to the fullerene (acceptor) [31–38].

Both of the PSs are characterized by a high quantum yield of the intersystem crossing process.

The combination of the chemical and photophysical properties of Ce6 and C_{60} could be a suitable strategy to obtain, in principle, an “ideal” photosensitizer that is able to bypass the limitations of the two molecules alone, including (i) poor cellular uptake for Ce6 and (ii) the lack of solubility in physiological environments and low absorption in the visible spectrum of C_{60} (chlorophylls are commonly used by nature as antenna molecules, and Ce6 is a chlorophyll-like donor).

Here, a novel procedure for the synthesis of a Ce6– C_{60} dyad is presented. The Ce6– C_{60} dyad was characterized from a chemical and photophysical point of view. The ability to generate ROS in physiological environments was investigated. The cellular uptake and the performance of the dyad in PDT were determined *in vitro*.

2. Results and Discussion

2.1. Synthesis and Characterization of the Ce6– C_{60} Dyad

The Ce6– C_{60} dyad was prepared via a coupling reaction between the carboxylic groups of the Ce6 molecule and a C_{60} derivative bearing an amine group (Figure 1). In brief, starting with ethylenediamine, a mono-protection with a Boc group was carried out, and the free amine was alkylated with benzyl bromoacetate. The deprotection of the carboxylic acid with a palladium on carbon mediated hydrogenation gave the α -amino acid **3**. A Prato reaction was carried out using **3** and formaldehyde to functionalize the C_{60} . The Boc protecting group was removed through an acid hydrolysis, obtaining the fullerene amino derivative **5**.

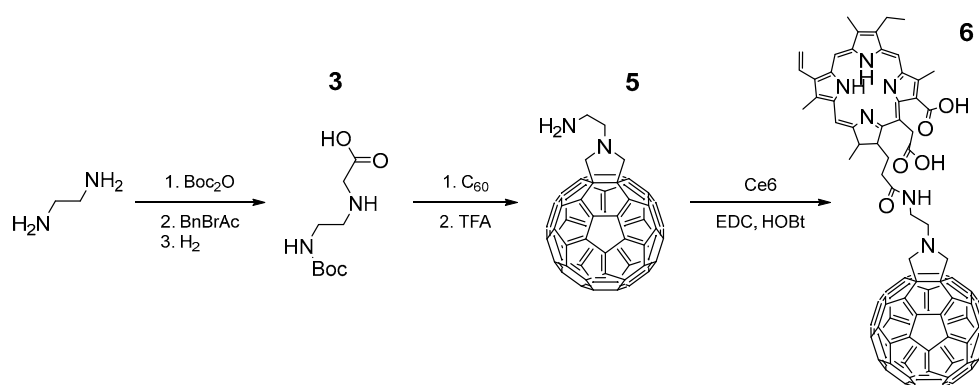


Figure 1. Synthesis of the Ce6– C_{60} (**6**) dyad.

An amidic coupling between **5** and Ce6 via EDC/HOBt activation gave the Ce6– C_{60} dyad (**6**). The mixture was purified using flash chromatography on silica gel, obtaining a dark-green to brownish solid.

Mass spectrometry (Figures S1 and S2) confirmed the covalent linkage of the dyad by the presence of a molecular peak with the expected isotopic pattern. The UV-Vis spectrum (Figure 2) of dyad **6** in DCM clearly showed both the diagnostic absorption bands of fullerene (256 nm and 324 nm) and Ce6 (406 and 668 nm).

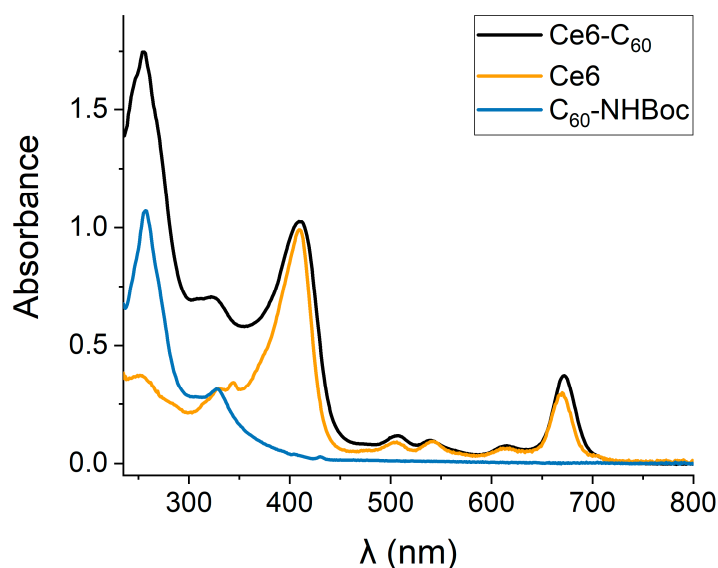


Figure 2. UV-Vis spectra of Ce6-C₆₀ (black line), Ce6 (gold line), and C₆₀-NHBoc (cyan line) in DCM.

Conjugation of the Ce6 with the fullerene derivative led to detectable changes in its absorption spectra; in particular, the red shift of the Q-band (3 nm in DCM, 5 nm in DMSO) and the broadening of the absorption bands were noticeable due to the interaction of Ce6 with the fullerene cage in the dyad, as was already reported for other fullerene–chlorin dyads [39].

Fluorescence quenching of Ce6 by the fullerene moiety was observed. As reported in Figure 3, upon excitation of the Q-band (at 500 nm), the emission band of the Ce6-C₆₀ dyad (centered at 670 nm) showed an intensity of about ten times lower ($\Phi_f = 0.015$) than an isoabsorbing solution of Ce6 ($\Phi_f = 0.17$) [40].

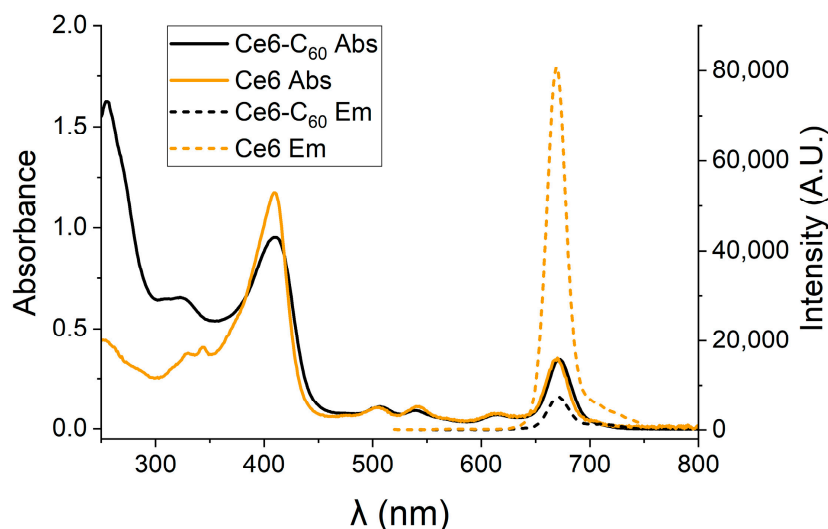


Figure 3. UV-Vis absorption spectra (solid lines) and emission spectra (dashed lines, $\lambda_{\text{ex}} = 500$ nm) of Ce6-C₆₀ (black lines) and Ce6 (gold lines).

This behavior is typical for fullerene–dye dyads, and it is due to the intramolecular energy or electron transfer from the donor (Ce6) to the fullerene acceptor, competing with the radiative deactivation of the Ce6 singlet excited state. The residual fluorescence of the dyad was particularly interesting for theranostic applications.

2.2. Generation of ROS by the Ce6–C₆₀ Dyad upon Red Light Irradiation

Ce6 is a well-known type II generator of ROS, characterized by the ability to produce singlet oxygen (¹O₂) upon red light irradiation. ABMDMA and Amplex Red assays, which determine, respectively, the generation of singlet oxygen (type II mechanism) and peroxides (type I mechanism), were used to investigate if the formation of the dyad affected the photosensitizing abilities of Ce6 upon red light irradiation. The Ce6–C₆₀ dyad showed a reduced ability in ¹O₂ production (type II mechanism) compared to the Ce6 alone (Figure 4A). The singlet oxygen quantum yield, which was calculated by using the ABMDMA assay (Figure S3), was 0.32 for the Ce6–C₆₀ dyad, which is about half of Ce6 alone ($\Phi_{\Delta} = 0.60$) [41,42]. On the other side, the production of peroxides (type I mechanism) was strongly improved, as expected from an antenna–fullerene system (Figure 4B) [38].

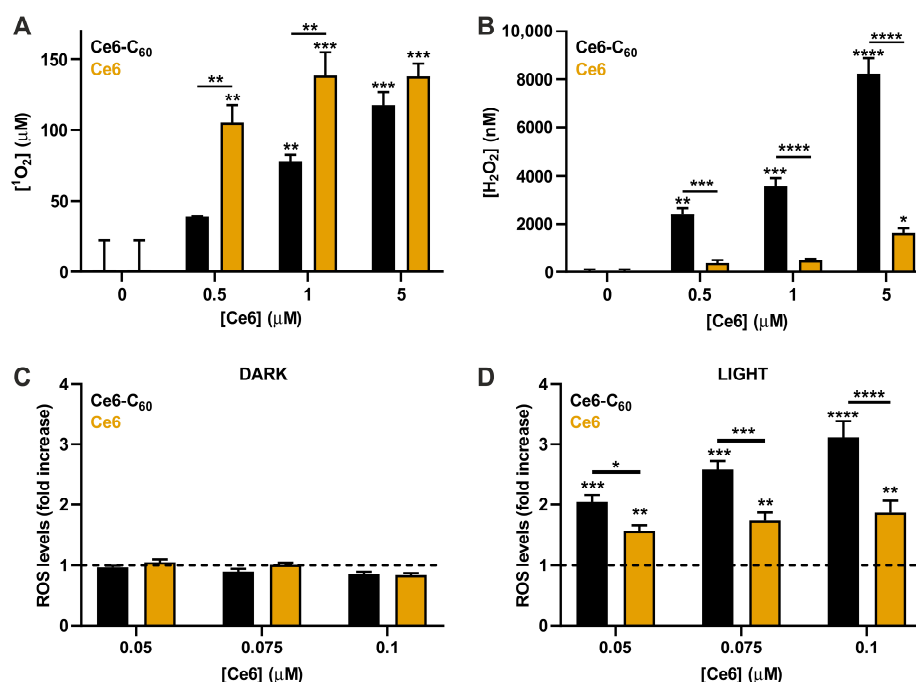


Figure 4. Quantification of ROS generated upon red light irradiation through (A) ABMDMA assay for the detection of ¹O₂ generated by the type II mechanism and (B) Amplex Red assay for the detection of H₂O₂ generated by the type I mechanism. Hydrogen peroxide levels were measured in cell cultures that were (C) kept in dark conditions or (D) irradiated with a red lamp through ROS-Glo™ H₂O₂ assay. Statistical significance was calculated using one-way ANOVA followed by Dunnett’s multiple comparisons. Stars above the bars indicate significance in comparison to the untreated control (0 μM), while the significance between Ce6 and Ce6–C₆₀ is indicated by stars above the line. * $p < 0.05$; ** $p < 0.01$; *** $p < 0.001$; **** $p < 0.0001$.

Intracellular production of ROS was also measured, confirming increased ROS production by the Ce6–C₆₀ dyad compared to Ce6 after PDT treatment in the A431 cells (Figure 4C,D).

This feature is very intriguing from an application standpoint, as PSs that produce ROS through the type I mechanism are more and more preferred in anticancer PDT [43–45] because they can overcome the hypoxic environment present in tumor tissues. This is because they rely less on oxygen content.

2.3. Cellular Uptake of the Ce6–C₆₀ Dyad

Ce6 bears three carboxylic side chains, and in physiological environments, it is negatively charged, limiting its cellular uptake. To improve the accumulation of Ce6 in cancer cells, two strategies are commonly pursued: (i) cationization of the Ce6 to improve the electrostatic interaction with the cellular membrane [46–49] and (ii) addition of a hydrophobic

moiety at the macrocycle periphery, with a high affinity towards cellular membranes [46,47] enhancing its ability to penetrate membranes and enter cells.

To assess the uptake of Ce6 and the Ce6–C₆₀ dyad, their internalization in A431 cells was quantitatively evaluated using flow cytometry analysis and recording the fluorescence signal of Ce6.

The data clearly show how the introduction of the hydrophobic fullerene moiety significantly improved the penetration of Ce6 through the cellular membrane, enhancing its uptake. In particular, after 3 h of incubation with 0.1 μM equimolar Ce6, a major difference was observed with a fluorescence increase of 12.8 ± 1.43 for Ce6–C₆₀ and 1.36 ± 1.21 for Ce6 (Figure 5). In brief, putting a ball and chain to chlorin e6, such as C₆₀, improves its cellular uptake.

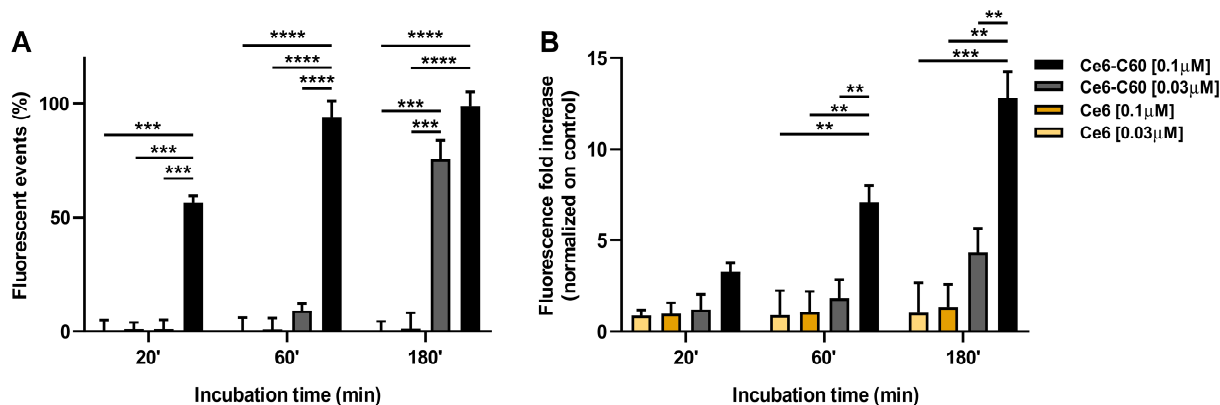


Figure 5. Cellular uptake of Ce6–C₆₀ and Ce6 vs. incubation time. (A) % of fluorescent events in comparison to the control. (B) Fold increase in the fluorescence intensity normalized on the control. A431 cell line was incubated with equimolar concentrations of Ce6, in particular with 0.1 μM (grey bars for Ce6–C₆₀ and yellow bars for Ce6) or 0.03 μM (black bars for Ce6–C₆₀ and gold bars for Ce6). Statistical significance was calculated using one-way ANOVA followed by Dunnett's multiple comparisons. ** $p < 0.01$; *** $p < 0.001$; **** $p < 0.0001$.

2.4. Phototoxicity of the Ce6–C₆₀ Dyad in A431 Cells Using Red Light Irradiation

Considering the outcomes of the internalization experiments, we investigated the phototoxic activity of Ce6 and the Ce6–C₆₀ dyad against A431 cells. No significant dark toxicity was observed for Ce6 or the Ce6–C₆₀ dyad until a concentration of 0.1 μM was reached (Figure 6). This aspect is extremely interesting because the conjugation of Ce6 to C₆₀ overcomes two significant restrictions on fullerene use in nanomedicine: (i) its lack of solubility in physiological environments and (ii) its low biocompatibility. Irradiation of the cells with a red lamp (45 min at 6.3 mW/cm², see Figure S4 for the spectral profile of the lamp) or with a laser (660 nm, 1 min, 2.66 W/cm²) showed an enhanced killing ability of the Ce6–C₆₀ dyad compared to Ce6 (Figure 6). The conjugation of C₆₀ to Ce6 caused a significant reduction in the viability of the A431 cells in a dose-dependent manner. Cell death after PDT treatment was confirmed by PI staining of the A431 cells. In both red-lamp and laser-irradiated samples, the presence of numerous PI-labeled cell nuclei was evident, demonstrating the cellular damage induced by the PDT treatment, which caused membrane permeabilization. Conversely, no PI-positive cells were observed in the samples that were kept in the dark (Figure 6D–I). In line with the uptake studies that demonstrate a greater internalization of Ce6–C₆₀, it appears that (i) the photokilling activity of the Ce6–C₆₀ dyad occurs at a lower concentration than Ce6 alone, and (ii) the PDT efficiency of Ce6–C₆₀ is approximately twice that of Ce6 ($69.01\% \pm 12.30\%$ for Ce6 and $28.82\% \pm 2.51\%$ for Ce6–C₆₀ after laser PDT treatment of samples incubated with the highest Ce6 concentration) (Figure 6).

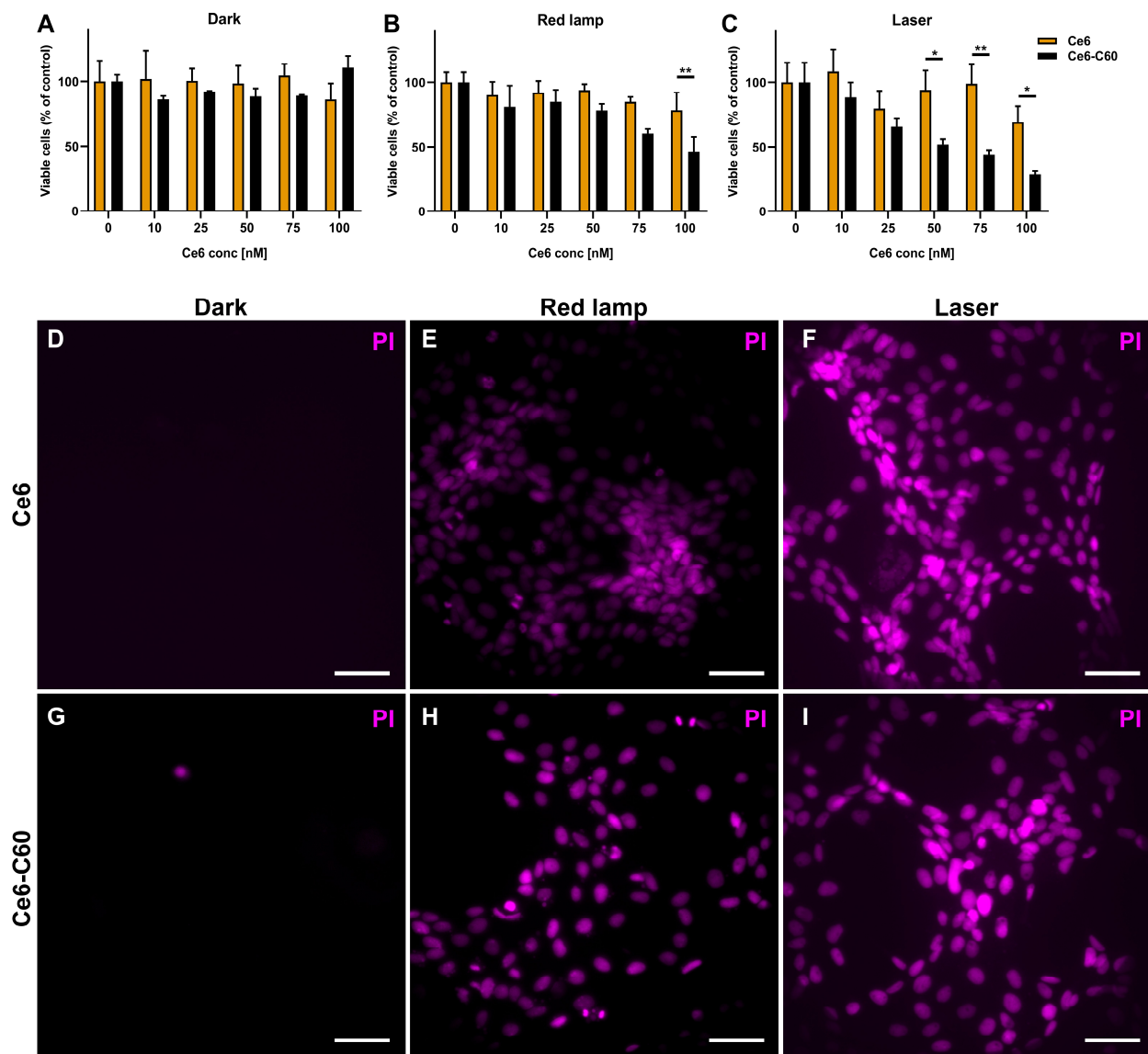


Figure 6. Cell viability of A431 cells after 24 h from PDT treatment with increasing concentrations of Ce6 (gold bars) or Ce6-C₆₀ (black bars). After incubation with the sensitizers, cells were (A) kept in dark conditions (control), (B) irradiated with red lamp, or (C) irradiated with laser. Propidium iodide staining of A431 cells incubated with Ce6 (D–F) or Ce6-C₆₀ (G–I) and kept in dark conditions (D,G), irradiated with red lamp (E,H), or irradiated with laser (F,I). Scale bar = 50 μm. Statistical significance was calculated using one-way ANOVA followed by Dunnett’s multiple comparisons test or t-test. * $p < 0.05$; ** $p < 0.01$.

3. Materials and Methods

3.1. Materials

Ethylenediamine ($\geq 99.5\%$), Di-tert-butyl dicarbonate (Boc₂O, $\geq 98.0\%$), Benzyl bromoacetate (96%), Triethylamine (TEA, $\geq 99\%$), Palladium on carbon (Pd/C, 10 wt.%), Fullerene-C₆₀ (98%), *N*-(3-Dimethylaminopropyl)-*N*'-ethylcarbodiimide hydrochloride (EDC, $\geq 98.0\%$), 1-Hydroxybenzotriazole hydrate (HOBt, $\geq 97.0\%$), 9,10-anthracenediylbis(methylene)dimalonic acid (ABMDMA), 10-Acetyl-3,7-dihydroxyphenoxazine (Amplex Red), and Type VI-A Peroxidase from horseradish lyophilized powder (HRP) were purchased from Merck (Darmstadt, Germany). Trifluoroacetic Acid (TFA, $\geq 99\%$) was purchased from TCI (Tokyo, Japan). Chlorin e6 (Ce6, $\geq 90\%$) was purchased from Cayman

Chemical (Ann Arbor, MI, USA). All the reagents were used without further purifications. Flash chromatography purifications were performed using Merck Geduran silica gel (40–63 μm particle size). Thin-layer chromatography analyses (TLC) were carried out by using Merck 60 F254 plates.

The ^1H and ^{13}C NMR spectra were recorded on a Varian INOVA 400 NMR instrument with a 5 mm probe. Chemical shifts (δ) were expressed in ppm and coupling constants (J) in Hertz (Hz).

HPLC-MS characterizations were carried out on an Agilent Technologies HP1260 instrument. A Phenomenex Gemini C18 3 μm (100 \times 3 mm) column was used for the chromatographic separation, with mobile-phase $\text{H}_2\text{O}/\text{CH}_3\text{CN}$, gradient of CH_3CN from 30% to 80% in 8 min, 80% CH_3CN until 22 min, then up to 90% CH_3CN in 2 min, flow rate of 0.4 mL/min. Mass spectrometric detection (ESI-MS) was performed in the full-scan mode from 50 to 3000 m/z using the following parameters: (i) scan time of 0.1 s, (ii) ESI spray voltage of 4000 V, (iii) nitrogen gas pressure of 30 psi, (iv) drying gas flow rate of 8.0 L/min, and (v) fragmentor voltage 30 V.

High-resolution MS (HR ESI-MS) characterizations were carried out with direct flow injection using a Xevo G2-XS ESI-QTOF mass spectrometer (Waters Corporation, Milford, Worcester, MA, USA). Mass spectrometric detection was performed in the full-scan mode from m/z 50 to 2000 using the following parameters: (i) scan time of 0.15 s in the positive ion mode with (ii) cone voltage of 30 V, (iii) capillary voltage of 3 kV, (iv) source temperature of 120 $^\circ\text{C}$, (v) desolvation temperature of 600 $^\circ\text{C}$, (vi) cone gas flow of 50 L/h, and (vii) desolvation gas flow of 1000 L/h. In the negative ion mode, the following parameters were used: (i) cone voltage of 45 V, (ii) capillary voltage of 2.5 kV, (iii) source temperature of 150 $^\circ\text{C}$, (iv) desolvation temperature of 350 $^\circ\text{C}$, (v) cone gas flow of 50 L/h, and (vi) desolvation gas flow of 800 L/h.

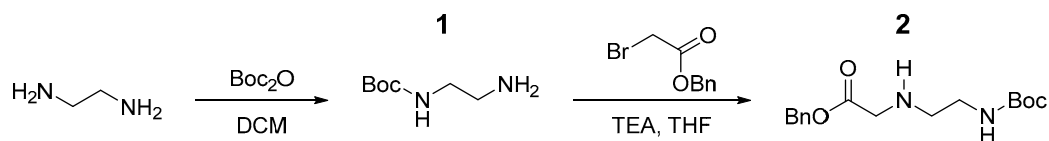
The absorption spectra were recorded using a Cary60 UV-Vis spectrophotometer (Agilent Technologies, Stockport, UK). The fluorescence spectra were recorded with an Edinburgh FLS920 equipped with a Hamamatsu R928P photomultiplier.

A LED SMD 50W RGB, SKU 5691, VT-4752 (V-TAC, Milan, Italy) was used as a red light source, with an irradiance of 6.32 mW/cm^2 and an emission band centered at 627 nm (Figure S4).

A 660 nm CW fiber-coupled infrared diode laser (FC-660, CNI Optoelectronics, Changchun, China) was used for the *in vitro* PDT treatment. The 660 nm laser was characterized by an irradiance of 2.66 W/cm^2 . The multiwell plate was perpendicular to the top-down, perpendicular laser irradiation.

3.2. Synthesis of Fullerene Derivative and Ce6–C₆₀ Dyad

Ethylenediamine (1.00 mL, 12.0 mmol) was dissolved in anhydrous dichloromethane (DCM, 15 mL) under a nitrogen atmosphere, and di-*tert*-butyl dicarbonate (Boc_2O , 873 mg, 4.00 mmol), which was previously dissolved in 5 mL of anhydrous DCM, was added dropwise at 0 $^\circ\text{C}$ (Scheme 1). After stirring at room temperature for 3 h, the mixture was checked by TLC (DCM:MeOH 9:1), and brine (20 mL) was added to the reaction solution. The extraction was carried out by using ethyl acetate (3 \times 20 mL), and then the combined organic fractions were dried over anhydrous sodium sulfate, and the filtrate concentrated in the vacuum. The crude product, obtained as a pale-yellow oil, was used without further purification.



Scheme 1. Synthesis of the intermediate 2.

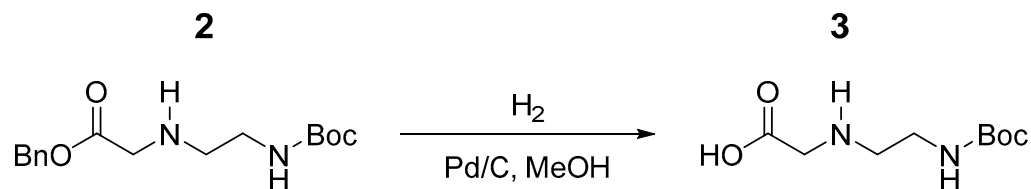
The crude mixture of **1** was dissolved in anhydrous tetrahydrofuran (THF, 8 mL) with triethylamine (TEA, 0.84 mL, 6 mmol) under a nitrogen atmosphere (Scheme 1). Lastly, benzyl bromoacetate (0.63 mL, 4 mmol) was added dropwise at 0 °C, observing the formation of a white solid. After stirring overnight at room temperature, water (20 mL) was added, and the mixture was extracted with ethyl acetate (3 × 20 mL), dried over anhydrous sodium sulfate, and the filtrate concentrated in vacuo. Column chromatography on silica gel (eluent: DCM:MeOH 98:2) gave the product **2** (666 mg, 2.16 mmol) as a yellowish oil in a 54% yield, as calculated over the two steps [50].

¹H NMR (400 MHz, Chloroform-*d*) (Figure S5): δ 7.40–7.31 (m, 5H), 5.17 (s, 2H), 5.05 (broad s, 1H), 3.48 (s, 2H), 3.23 (q, *J* = 5.3 Hz, 2H), 2.78 (t, *J* = 5.7 Hz, 2H), 1.44 (s, 9H).

¹³C NMR (100 MHz, Chloroform-*d*) (Figure S6): δ 172.4, 156.0, 135.5, 128.6, 128.4, 128.3, 77.2, 66.6, 50.5, 48.7, 40.1, 28.4.

HPLC-MS (Acetonitrile) (Figure S7) Rt: 5.63 min, [M+H]⁺ 309.40.

Pd/C (10 wt. %, 106 mg, 0.10 mmol) was added to an anhydrous methanol solution (5 mL) of **2** (308 mg, 1 mmol), and the mixture was stirred overnight under a hydrogen atmosphere (Scheme 2). Celite filtration removed the catalyst, and then the solvent was evaporated. The product was washed with diethyl ether to give a white solid (176 mg, 0.81 mmol) in 81% yield.



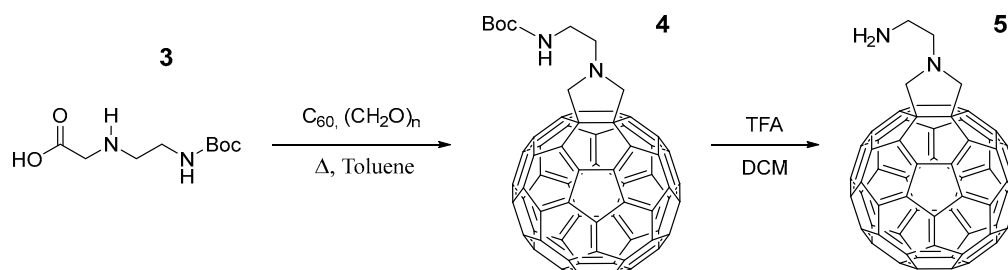
Scheme 2. Synthesis of intermediate **3**.

¹H NMR (400 MHz, CD₃OD) (Figure S8): δ 3.49 (s, 2H), 3.35 (t, *J* = 5.9 Hz, 2H), 3.09 (t, *J* = 5.9 Hz, 2H), 1.43 (s, 9H).

¹³C NMR (100 MHz, CD₃OD) (Figure S9): δ 170.7, 158.7, 80.8, 50.6, 48.9, 38.1, 28.7.

HPLC-MS (Acetonitrile) (Figure S10) Rt: 1.28 min, [M+H]⁺ 219.20.

A toluene solution (120 mL) of C₆₀ (248 mg, 0.34 mmol), paraformaldehyde (21 mg, 0.69 mmol), and amino acid **3** (60 mg, 0.28 mmol) was heated to reflux for 1 h under a nitrogen atmosphere (Scheme 3). After cooling to room temperature and checking the formation of a brown spot with TLC (toluene:AcOEt 95:5), the product was purified on silica gel using column chromatography, first eluting it with toluene to recover the unreacted C₆₀ and then with toluene:AcOEt 97:3 to separate the mono from the bis-adducts. The brown solid was thoroughly washed with diethyl ether to obtain a pure product (65 mg, 72 μmol) in a 26% yield [51].



Scheme 3. Synthesis of intermediate **5**.

¹H NMR (400 MHz, Chloroform-*d*:CS₂ 1:1) (Figure S11) δ 5.27 (broad s, 1H), 4.51 (s, 4H), 3.72 (q, *J* = 5.8 Hz, 2H), 3.30 (t, *J* = 6.0 Hz, 2H), 1.54 (s, 9H).

HR ESI-MS (MeOH) (Figures S12 and S13): [M+H]⁺ 907.1178, [M+Na]⁺ 929.0993.

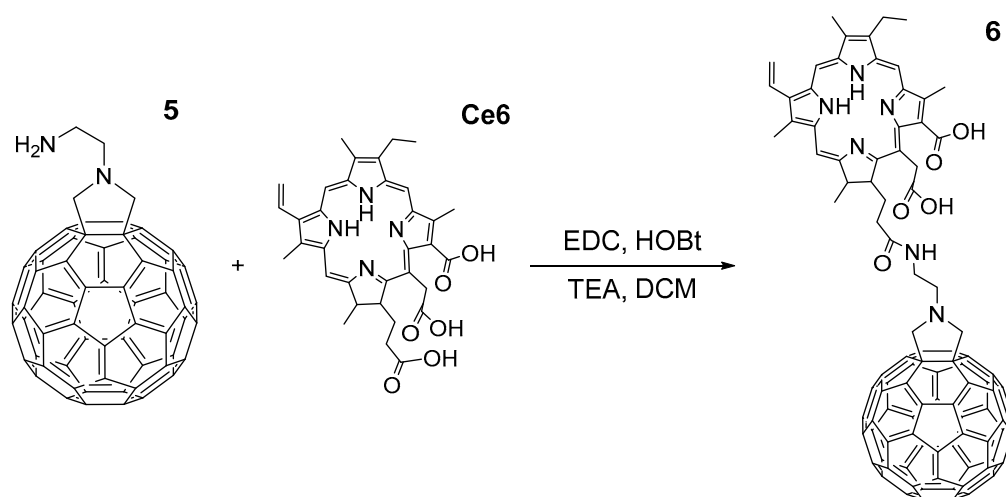
UV-Vis (DCM) (Figure S14) λ_{max} 430 nm, 327 nm, 257 nm.

A solution of **4** (65 mg, 72 μmol) in DCM (1 mL) and trifluoroacetic acid (1 mL) was stirred at room temperature for 3 h (Scheme 3). The solvent and the acid in excess were removed in vacuo, obtaining the product as an ammonium salt ($\text{C}_{60}\cdot\text{TFA}$) and as a brown solid (70 mg, 68 μmol) in a 94% yield.

ESI-MS (MeOH) (Figure S15): $[\text{M}+\text{H}]^+$ 806.98.

UV-Vis (DMSO) (Figure S16): λ_{max} 433 nm, 325 nm.

Chlorin e6 (23 μmol , 14 mg), EDC·HCl (46 μmol , 9 mg), and HOBT (46 μmol , 6 mg) were dissolved in anhydrous DCM (5 mL) and stirred at room temperature for 1 h. This solution was added dropwise to a suspension of the fullerene derivative **5** (23 μmol , 24 mg) and TEA (46 μmol , 6 μL) in anhydrous DCM (10 mL) (Scheme 4). The resulting reaction mixture was stirred overnight at room temperature under a nitrogen atmosphere. The solvent was then evaporated under reduced pressure, and the product was purified using flash chromatography on silica gel using 95:5 DCM/MeOH as eluent. Successive washing with diethyl ether (3×5 mL) gave the product as a dark-green to brownish solid (7 mg, 5 μmol) in a 21% yield.



Scheme 4. Amide coupling for the synthesis of the Ce6-C₆₀ dyad.

HR ESI-MS (MeOH) (Figures S1 and S2): $[\text{M}-\text{H}]^-$ 1383.3271, $[\text{M}-\text{CO}_2]^-$ 1339.3300, $[\text{M}+\text{OH}]^-$ 1400.3185, $[\text{M}+\text{CH}_3\text{O}]^-$ 1414.3060.

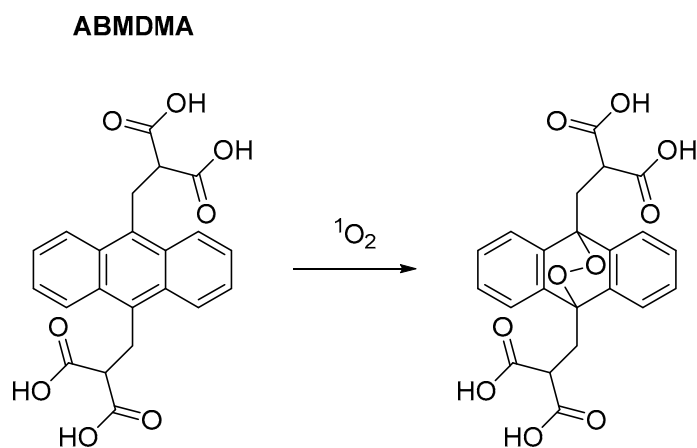
UV-Vis (DCM): λ_{max} 672 nm, 615 nm, 539 nm, 506 nm, 409 nm, 322 nm, 255 nm.

¹H NMR (400 MHz, Chloroform-*d*): δ 9.63 (s, 1H), 9.51 (s, 1H), 8.61 (s, 1H), 7.97 (dd, $J = 17.8, 11.4$ Hz, 1H), 6.26 (dd, $J = 17.9, 1.6$ Hz, 1H), 6.14 (dd, $J = 11.5, 1.4$ Hz, 1H), 4.44 (s, 4H), 4.15–4.05 (m, 2H), 4.04–3.93 (m, 2H), 3.80 (m, 6H), 3.36 (m, 3H), 3.26 (m, 6H), 3.19 (s, 1H), 2.62–2.52 (m, 2H), 2.35 (q, $J = 7.6$ Hz, 1H), 1.76–1.62 (m, 6H).

3.3. Detection of ROS Produced upon Red Light Irradiation

ABMDMA assay. 9,10-Anthracenediyl-bis(methylene)dimalonic acid (ABMDMA) was used as singlet oxygen detector. The disodium salt of ABMDMA reacts with ¹O₂ to give an endoperoxide (Scheme 5), which is detected as a decline of the absorbance at 401 nm [52,53].

DMSO stock solutions of Ce6 and Ce6-C₆₀ were prepared with concentrations of 100, 20, and 10 μM , as determined from the Ce6 molar extinction coefficient at 670 nm. In a 96-well plate, 5 μL of these solutions were added to 95 μL of deuterated PBS (10 mM pH 7.4) in order to test the final concentrations of 5, 1, and 0.5 μM . Another well was filled with only deuterated PBS and DMSO (5%). Lastly, 3 μL of an ABMDMA 5 mM stock solution in DMSO was added to each well. The plate was irradiated for 1 h with a red light lamp.



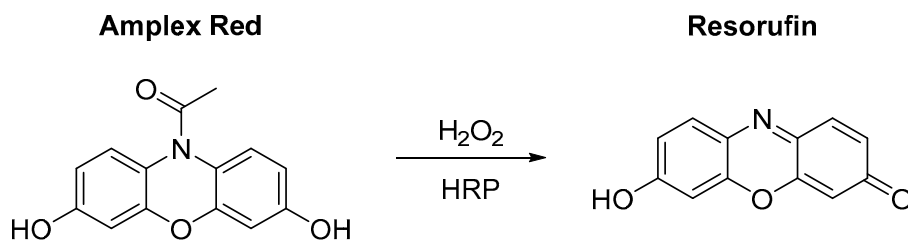
Scheme 5. Reaction scheme of ABMDMA with singlet oxygen.

The singlet oxygen quantum yield (Φ_{Δ}) of Ce6 and Ce6–C₆₀ was determined by irradiating the samples with the red lamp for up to 20 min and following the ABMDMA bleaching over time, with timesteps of 5 min. The Φ_{Δ} was calculated using the following equation:

$$\Phi_{\Delta}^{\text{Ce6-C60}} = \frac{k^{\text{Ce6-C60}}}{k^{\text{Ce6}}} \times \Phi_{\Delta}^{\text{Ce6}} \quad (1)$$

where k is the slope of the photooxidation rate of ABMDMA obtained by the curve-fitting equation (Figure S3). Absorbance data were collected before and after the irradiation using a PerkinElmer EnSpire[®] Multimode Plate Reader (Cambridge, MA, USA).

Amplex Red assay. The Amplex Red (AR) assay was used to evaluate the generation of peroxides upon irradiation with visible light. Colorless and nonfluorescent Amplex Red reacts with peroxides in a reaction catalyzed by horseradish peroxidase (HRP) to form Resorufin, which is a fluorescent molecule (Scheme 6) [10,54].



Scheme 6. Reaction scheme of Amplex Red with hydrogen peroxide.

The concentration of the produced peroxides was calculated by measuring the fluorescence emission of Resorufin at 590 nm (excitation at 560 nm), subtracting the values of non-irradiated references that were kept in the dark. The fluorescence values were converted into hydrogen peroxide concentrations using a calibration curve obtained from standard solutions of H₂O₂. 10 μ L of 50 mM AR stock solution in DMSO was diluted in 1 mL of 50 mM phosphate buffer at pH 7.4 (PB) to obtain a solution characterized by a final AR concentration of 500 μ M. The final working solution (WS) was obtained by adding 10 μ L of HRP at 0.4 mg/mL in PB to the AR solution. Stock solutions of Ce6 and Ce6–C₆₀ in DMSO were prepared, with concentrations of 100, 20, and 10 μ M. In a 96-well plate, 5 μ L of these solutions was added to 85 μ L of PB (final concentrations of Ce6 and Ce6–C₆₀ of 5, 1, and 0.5 μ M). The plate was irradiated with a red light lamp for 1 h and then 10 μ L of the WS was added to each well. An equivalent plate was kept in the dark and then the WS was added. After 30 min, the fluorescence data were collected using a PerkinElmer EnSpire[®] Multimode Plate Reader (Cambridge, MA, USA).

Intracellular ROS Production. Intracellular ROS production after PDT was determined by using ROS-Glo™ H₂O₂ Assay (Promega, Madison, WI, USA), following the protocol provided by the manufacturer. Briefly, around 25,000 A431 cells (ATCC CRL-1555) were incubated for 3 h with increasing concentrations of either Ce6 or Ce6–C₆₀ prior to washing and irradiation with a red light lamp for 45 min. Immediately after the treatment, 20 µL of H₂O₂ substrate solution was added to each well (final volume 100 µL) and incubated for 20 min at 37 °C. A total of 100 µL of ROS-Glo™ detection solution was added to each sample, and the plate was incubated at room temperature for 20'. Relative luminescence was measured using EnSpire® multimode plate reader (PerkinElmer, Cambridge, MA, USA).

3.4. Cellular Uptake

Cellular uptake of Ce6–C₆₀ and Ce6 was evaluated on an A431 human epidermal carcinoma cell line (ATCC CRL-1555). A total of 100,000 cells were seeded in a 6-well plate and incubated overnight at 37 °C with 5% CO₂. Next, cells were incubated with either 0.1 µM or 0.03 µM concentrations of Ce6–C₆₀ or Ce6 for 20, 60, or 180 min. After the incubation, cells were washed twice with PBS to remove any unbound sensitizers. Subsequently, the cells were detached by trypsinization and analyzed using a citoFLEX S flow cytometer (Beckman Coulter, Brea, CA, USA). Data analysis was performed using CytExpert software 2.5 (Beckman Coulter) and FlowJo™ 10.9 software.

3.5. Cytotoxicity and Phototoxicity in A431 Cells

MTT assay. In a 96-well flat-bottom plate (Sarstedt, Germany), 25,000 cells of confluent growing A431 cells were seeded in 100 µL complete growth media RPMI (10% FBS, 1% L-Glutamine, 1% Penicillin-Streptomycin) per well and incubated overnight at 37 °C with 5% CO₂. Cells were then incubated with increasing concentrations of Ce6 or Ce6–C₆₀ (diluted in RPMI) for 3 h at 37 °C with 5% CO₂. Afterwards, cells were washed twice with 1× PBS to remove any free sensitizer. For irradiation, 100 µL of 1× PBS was added per well, and the 96-well plate was irradiated for 45 min with a red lamp (6.3 mW/cm², see Figure S4 for the spectral profile of the lamp) or a laser (660 nm, 2.66 W/cm²) for 1 min per well.

Cells were allowed to recover overnight in 200 µL complete RPMI per well at 37 °C with 5% CO₂. The dark control plate was treated the same way but kept in the dark throughout. The cell viability was tested using MTT assay. Therefore, the cells were incubated in a final concentration of 0.5 mg/mL MTT (Sigma-Aldrich, St. Louis, MO, USA) in 100 µL RPMI per well for 90 min at 37 °C with 5% CO₂. Next, the media were removed, and 100 µL per well of DMSO was added for the formazan solubilization. To determine the cell viability, the absorbance was measured at 570 and 690 nm wavelengths using the EnSpire multimode plate reader (PerkinElmer, Cambridge, MA, USA), and the absorbance at 570 nm was subtracted from the absorbance at 690 nm. The obtained values were normalized against a growth control that was not treated with sensitizer. The results are shown as the mean ± SD of three biological replicates, each with three technical replicates.

Propidium iodide staining. A431 cells were seeded on round coverslips placed inside a 6-well plate (Corning) and grown overnight at 37 °C with 5% CO₂. Cells were then incubated in MTT assay, as described above, with either Ce6 or Ce6–C₆₀ at a final Ce6 equimolar concentration of 0.1 µM and (i) kept in dark conditions, (ii) irradiated for 45 min with a red lamp (6.3 mW/cm²), or (iii) irradiated for 1 min with laser at 660 nm (2.66 W/cm²). Cells were then recovered for 24 h and stained for 30 min with Propidium iodide (PI) at a final concentration of 1 µM. A round coverslip was fitted into an Attofluor cell chamber (Invitrogen, Carlsbad, CA, USA) and covered with 1 mL of RPMI without phenol red complete (10% FBS, 1% PenStrep, and 1% L-glutamine). Cell images were then acquired with a Nikon Eclipse Ti-U inverted epifluorescence microscope.

4. Conclusions

In summary, we developed a novel phototheranostic platform for PDT treatment/fluorescence imaging based on the Ce6–C₆₀ dyad. The Ce6–C₆₀ dyad was synthesized via a coupling reaction between the carboxylic groups of the Ce6 molecule and a C₆₀ derivative bearing an amine group.

Combining the peculiar properties of Ce6 and C₆₀, the obtained Ce6–C₆₀ dyad had the following characteristics: (i) efficient absorption in the red region of the visible spectrum; (ii) production of ROS following both type I and type II photophysical mechanisms; (iii) good biocompatibility and solubility in physiological environments; (iv) enhanced cellular uptake efficiency in vitro (with a fluorescence increase of 10.5 times after 3 h of incubation in comparison to Ce6); (v) simultaneous imaging capability and PDT performances. Remarkably, the dyad displayed superior photo-capabilities in terms of both peroxide generation and PDT efficiency on cancer cells. Notably, dyad irradiation resulted in the production of five times more peroxides and the photokilling of 40.2% more cancer cells compared to Ce6 at the same equimolar concentration.

This approach paves the way for the molecular engineering of highly efficient fullerene-based photosensitizers for anticancer PDT. The unique properties of the Ce6–C₆₀ dyad suggest that, in perspective, it can be used as a new red light phototheranostic agent for fluorescence-imaging-guided PDT treatment.

Supplementary Materials: The following supporting information can be downloaded at <https://www.mdpi.com/article/10.3390/ph16091329/s1>, Figures S1 and S2: HR ESI-MS of compound 6; Figure S3: Absorbance of ABMDMA vs. irradiation time; Figure S4: Spectral profile of the red light lamp; Figure S5: ¹H NMR of compound 2; Figure S6: ¹³C NMR of compound 2; Figure S7: HPLC-MS of compound 2; Figure S8: ¹H NMR of compound 3; Figure S9: ¹³C NMR of compound 3; Figure S10: HPLC-MS of compound 3; Figure S11: ¹H NMR of compound 4; Figure S12: HR ESI-MS of compound 4; Figure S13: HR ESI-MS of compound 4; Figure S14: UV-Vis spectrum of compound 4; Figure S15: ESI-MS of compound 5; Figure S16: UV-Vis spectrum of compound 5.

Author Contributions: Conceptualization, M.C.; methodology, P.E.C. and M.D.G.; formal analysis, M.D.S., A.K., M.L., A.D., P.E.C. and M.D.G.; investigation, M.D.S. and A.K.; resources, M.L., A.D. and M.C.; writing—review and editing, all authors; supervision, M.L., A.D. and M.C.; funding acquisition, M.C. All authors have read and agreed to the published version of the manuscript.

Funding: The research leading to these results received funding from AIRC under the MFAG 2019 ID. 22894 project (P.I.: M.C.).

Institutional Review Board Statement: Not applicable.

Informed Consent Statement: Not applicable.

Data Availability Statement: Data is contained within the article and supplementary material.

Conflicts of Interest: The authors declare no conflict of interest.

References

1. Ormond, A.B.; Freeman, H.S. Dye Sensitizers for Photodynamic Therapy. *Materials* **2013**, *6*, 817–840. [[CrossRef](#)] [[PubMed](#)]
2. Lan, M.; Zhao, S.; Liu, W.; Lee, C.S.; Zhang, W.; Wang, P. Photosensitizers for Photodynamic Therapy. *Adv. Healthc. Mater.* **2019**, *8*, 1900132. [[CrossRef](#)] [[PubMed](#)]
3. Hak, A.; Ali, M.S.; Sankaranarayanan, S.A.; Shinde, V.R.; Rengan, A.K. Chlorin E6: A Promising Photosensitizer in Photo-Based Cancer Nanomedicine. *ACS Appl. Bio Mater.* **2023**, *6*, 349–364. [[CrossRef](#)]
4. Liao, S.; Cai, M.; Zhu, R.; Fu, T.; Du, Y.; Kong, J.; Zhang, Y.; Qu, C.; Dong, X.; Ni, J.; et al. Antitumor Effect of Photodynamic Therapy/Sonodynamic Therapy/Sono-Photodynamic Therapy of Chlorin e6 and Other Applications. *Mol. Pharm.* **2023**, *20*, 875–885. [[CrossRef](#)] [[PubMed](#)]
5. Juzienne, A. Chlorin E6-Based Photosensitizers for Photodynamic Therapy and Photodiagnosis. *Photodiagnosis Photodyn. Ther.* **2009**, *6*, 94–96. [[CrossRef](#)]
6. Sharma, S.K.; Chiang, L.Y.; Hamblin, M.R. Photodynamic Therapy with Fullerenes in Vivo: Reality or a Dream? *Nanomedicine* **2011**, *6*, 1813–1825. [[CrossRef](#)]

7. Mroz, P.; Tegos, G.P.; Gali, H.; Wharton, T.; Sarna, T.; Hamblin, M.R. Photodynamic Therapy with Fullerenes. *Photochem. Photobiol. Sci.* **2007**, *6*, 1139–1149. [[CrossRef](#)]
8. Hamblin, M.R. Fullerenes as Photosensitizers in Photodynamic Therapy: Pros and Cons. *Photochem. Photobiol. Sci.* **2018**, *17*, 1515–1533. [[CrossRef](#)]
9. Hou, W.; Shi, G.; Wu, S.; Mo, J.; Shen, L.; Zhang, X.; Zhu, Y. Application of Fullerenes as Photosensitizers for Antimicrobial Photodynamic Inactivation: A Review. *Front. Microbiol.* **2022**, *13*, 957698. [[CrossRef](#)]
10. Cantelli, A.; Malferrari, M.; Mattioli, E.J.; Marconi, A.; Mirra, G.; Soldà, A.; Marforio, T.D.; Zerbetto, F.; Rapino, S.; Di Giosia, M.; et al. Enhanced Uptake and Phototoxicity of C60@albumin Hybrids by Folate Bioconjugation. *Nanomaterials* **2022**, *12*, 3501. [[CrossRef](#)]
11. Di Giosia, M.; Nicolini, F.; Ferrazzano, L.; Soldà, A.; Valle, F.; Cantelli, A.; Marforio, T.D.; Bottoni, A.; Zerbetto, F.; Montalti, M.; et al. Stable and Biocompatible Monodispersion of C60 in Water by Peptides. *Bioconjugate Chem.* **2019**, *30*, 808–814. [[CrossRef](#)]
12. Di Giosia, M.; Soldà, A.; Seeger, M.; Cantelli, A.; Arnesano, F.; Nardella, M.I.; Mangini, V.; Valle, F.; Montalti, M.; Zerbetto, F.; et al. A Bio-Conjugated Fullerene as a Subcellular-Targeted and Multifaceted Phototheranostic Agent. *Adv. Funct. Mater.* **2021**, *31*, 2101527. [[CrossRef](#)]
13. Serda, M.; Szewczyk, G.; Krzysztżyńska-Kuleta, O.; Korzuch, J.; Dulski, M.; Musioł, R.; Sarna, T. Developing [60]Fullerene Nanomaterials for Better Photodynamic Treatment of Non-Melanoma Skin Cancers. *ACS Biomater. Sci. Eng.* **2020**, *6*, 5930–5940. [[CrossRef](#)] [[PubMed](#)]
14. Serda, M.; Ware, M.J.; Newton, J.M.; Sachdeva, S.; Krzykawska-Serda, M.; Nguyen, L.; Law, J.; Anderson, A.O.; Curley, S.A.; Wilson, L.J.; et al. Development of Photoactive Sweet-C 60 for Pancreatic Cancer Stellate Cell Therapy. *Nanomedicine* **2018**, *13*, 2981–2993. [[CrossRef](#)] [[PubMed](#)]
15. Antoku, D.; Sugikawa, K.; Ikeda, A. Photodynamic Activity of Fullerene Derivatives Solubilized in Water by Natural-Product-Based Solubilizing Agents. *Chem. A Eur. J.* **2019**, *25*, 1854–1865. [[CrossRef](#)] [[PubMed](#)]
16. Vicente, M.d.G.H.; Smith, K.M. Amino Acid Derivatives of Chlorin-E6—A Review. *Molecules* **2023**, *28*, 3479. [[CrossRef](#)]
17. Osaki, T.; Hibino, S.; Yokoe, I.; Yamaguchi, H.; Nomoto, A.; Yano, S.; Mikata, Y.; Tanaka, M.; Kataoka, H.; Okamoto, Y. A Basic Study of Photodynamic Therapy with Glucose-Conjugated Chlorin E6 Using Mammary Carcinoma Xenografts. *Cancers* **2019**, *11*, 63. [[CrossRef](#)]
18. Shinoda, Y.; Kujirai, K.; Aoki, K.; Morita, M.; Masuda, M.; Zhang, L.; Kaixin, Z.; Nomoto, A.; Takahashi, T.; Tsuneoka, Y.; et al. Novel Photosensitizer β -Mannose-Conjugated Chlorin E6 as a Potent Anticancer Agent for Human Glioblastoma U251 Cells. *Pharmaceuticals* **2020**, *13*, 316. [[CrossRef](#)]
19. Thapa Magar, T.B.; Lee, J.; Lee, J.H.; Jeon, J.; Gurung, P.; Lim, J.; Kim, Y.-W. Novel Chlorin E6-Curcumin Derivatives as a Potential Photosensitizer: Synthesis, Characterization, and Anticancer Activity. *Pharmaceutics* **2023**, *15*, 1577. [[CrossRef](#)]
20. Qin, X.; Zhang, M.; Hu, X.; Du, Q.; Zhao, Z.; Jiang, Y.; Luan, Y. Nanoengineering of a Newly Designed Chlorin E6 Derivative for Amplified Photodynamic Therapy: Via Regulating Lactate Metabolism. *Nanoscale* **2021**, *13*, 11953–11962. [[CrossRef](#)]
21. Dias, L.D.; Mfouo-Tynga, I.S. Learning from Nature: Bioinspired Chlorin-Based Photosensitizers Immobilized on Carbon Materials for Combined Photodynamic and Photothermal Therapy. *Biomimetics* **2020**, *5*, 53. [[CrossRef](#)] [[PubMed](#)]
22. Marconi, A.; Mattioli, E.J.; Ingargiola, F.; Giugliano, G.; Marforio, D.; Prodi, L.; Di Giosia, M.; Calvaresi, M. Dissecting the Interactions between Chlorin E6 and Human Serum Albumin. *Molecules* **2023**, *28*, 2348. [[CrossRef](#)] [[PubMed](#)]
23. Lim, C.; Kang, J.K.; Won, W.R.; Park, J.Y.; Han, S.M.; Le, T.N.; Kim, J.C.; Her, J.; Shin, Y.; Oh, K.T. Co-Delivery of D-(KLAKLAK)₂ Peptide and Chlorin E6 Using a Liposomal Complex for Synergistic Cancer Therapy. *Pharmaceutics* **2019**, *11*, 293. [[CrossRef](#)] [[PubMed](#)]
24. Park, C.; Yoo, J.; Lee, D.; Jang, S.Y.; Kwon, S.; Koo, H. Chlorin E6-Loaded PEG-PCL Nanoemulsion for Photodynamic Therapy and in vivo Drug Delivery. *Int. J. Mol. Sci.* **2019**, *20*, 3958. [[CrossRef](#)]
25. Peng, P.C.; Hong, R.L.; Tsai, T.; Chen, C.T. Co-Encapsulation of Chlorin E6 and Chemotherapeutic Drugs in a Pegylated Liposome Enhance the Efficacy of Tumor Treatment: Pharmacokinetics and Therapeutic Efficacy. *Pharmaceutics* **2019**, *11*, 617. [[CrossRef](#)]
26. Sundaram, P.; Abrahamse, H. Effective Photodynamic Therapy for Colon Cancer Cells Using Chlorin E6 Coated Hyaluronic Acid-Based Carbon Nanotubes. *Int. J. Mol. Sci.* **2020**, *21*, 4745. [[CrossRef](#)]
27. Nasr, S.; Rady, M.; Sebak, A.; Gomaa, I.; Fayad, W.; El Gaafary, M.; Abdel-kader, M.; Syrovets, T.; Simmet, T. A Naturally Derived Carrier for Photodynamic Treatment of Squamous Cell Carcinoma: In Vitro and in Vivo Models. *Pharmaceutics* **2020**, *12*, 494. [[CrossRef](#)]
28. Montellano, A.; Da Ros, T.; Bianco, A.; Prato, M. Fullerene C60 as a Multifunctional System for Drug and Gene Delivery. *Nanoscale* **2011**, *3*, 4035–4041. [[CrossRef](#)]
29. Goodarzi, S.; Da Ros, T.; Conde, J.; Sefat, F.; Mozafari, M. Fullerene: Biomedical Engineers Get to Revisit an Old Friend. *Mater. Today* **2017**, *20*, 460–480. [[CrossRef](#)]
30. Kazemzadeh, H.; Mozafari, M. Fullerene-Based Delivery Systems. *Drug Discov. Today* **2019**, *24*, 898–905. [[CrossRef](#)]
31. Antoku, D.; Satake, S.; Mae, T.; Sugikawa, K.; Funabashi, H.; Kuroda, A.; Ikeda, A. Improvement of Photodynamic Activity of Lipid-Membrane-Incorporated Fullerene Derivative by Combination with a Photo-Antenna Molecule. *Chem. A Eur. J.* **2018**, *24*, 7335–7339. [[CrossRef](#)] [[PubMed](#)]

32. Shimada, R.; Hino, S.; Yamana, K.; Kawasaki, R.; Konishi, T.; Ikeda, A. Improvement of Photodynamic Activity by a Stable System Consisting of a C60 Derivative and Photoantenna in Liposomes. *ACS Med. Chem. Lett.* **2022**, *13*, 641–647. [[CrossRef](#)] [[PubMed](#)]
33. Kawasaki, R.; Antoku, D.; Ohdake, R.; Sugikawa, K.; Ikeda, A. Bacterial Elimination via the Photodynamic Activity of a Fullerene/Light-Harvesting Antenna Molecule Assembled System Integrated into Liposome Membranes. *Nanoscale Adv.* **2020**, *2*, 4395–4399. [[CrossRef](#)] [[PubMed](#)]
34. Gonzalez Lopez, E.J.; Sarotti, A.M.; Martínez, S.R.; Macor, L.P.; Durantini, J.E.; Renfige, M.; Gervaldo, M.A.; Otero, L.A.; Durantini, A.M.; Durantini, E.N.; et al. BOPHY-Fullerene C60 Dyad as a Photosensitizer for Antimicrobial Photodynamic Therapy. *Chem. A Eur. J.* **2022**, *28*, e202103884. [[CrossRef](#)] [[PubMed](#)]
35. Guan, M.; Ge, J.; Wu, J.; Zhang, G.; Chen, D.; Zhang, W.; Zhang, Y.; Zou, T.; Zhen, M.; Wang, C.; et al. Fullerene/Photosensitizer Nanovesicles as Highly Efficient and Clearable Phototheranostics with Enhanced Tumor Accumulation for Cancer Therapy. *Biomaterials* **2016**, *103*, 75–85. [[CrossRef](#)]
36. Agazzi, M.L.; Almodovar, V.A.S.; Gsponer, N.S.; Bertolotti, S.; Tomé, A.C.; Durantini, E.N. Diketopyrrolopyrrole-Fullerene C60 Architectures as Highly Efficient Heavy Atom-Free Photosensitizers: Synthesis, Photophysical Properties and Photodynamic Activity. *Org. Biomol. Chem.* **2020**, *18*, 1449–1461. [[CrossRef](#)]
37. Rybkin, A.Y.; Belik, A.Y.; Goryachev, N.S.; Mikhaylov, P.A.; Kraevaya, O.A.; Filatova, N.V.; Parkhomenko, I.I.; Peregudov, A.S.; Terent'ev, A.A.; Larkina, E.A.; et al. Self-Assembling Nanostructures of Water-Soluble Fullerene [60]–Chlorin E6 Dyads: Synthesis, Photophysical Properties, and Photodynamic Activity. *Dyes Pigments* **2020**, *180*, 108411. [[CrossRef](#)]
38. Li, Q.; Huang, C.; Liu, L.; Hu, R.; Qu, J. Enhancing Type I Photochemistry in Photodynamic Therapy under Near Infrared Light by Using Antennae–Fullerene Complexes. *Cytom. Part A* **2018**, *93*, 997–1003. [[CrossRef](#)]
39. Bertran, J.C.; Montforts, F.P. Synthesis of a Chlorin Fullerene Dyad for Artificial Photosynthesis. *Eur. J. Org. Chem.* **2017**, *12*, 1608–1617. [[CrossRef](#)]
40. Di Giosia, M.; Genovese, D.; Cantelli, A.; Cingolani, M.; Rampazzo, E.; Strever, G.; Tavoni, M.; Zaccheroni, N.; Calvaresi, M.; Prodi, L. Synthesis and Characterization of a Reconstituted Myoglobin-Chlorin E6 Adduct for Theranostic Applications. *J. Porphyr. Phthalocyanines* **2020**, *24*, 887–893. [[CrossRef](#)]
41. Redmond, R.W.; Gamlin, J.N. A Compilation of Singlet Oxygen Yields from Biologically Relevant Molecules. *Photochem. Photobiol.* **1999**, *70*, 391–475. [[CrossRef](#)] [[PubMed](#)]
42. Parkhats, M.V.; Galievsky, V.A.; Stashevsky, A.S.; Trukhacheva, T.V.; Dzhagarov, B.M. Dynamics and Efficiency of the Photosensitized Singlet Oxygen Formation by Chlorin E6: The Effects of the Solution PH and Polyvinylpyrrolidone. *Opt. Spectrosc.* **2009**, *107*, 974–980. [[CrossRef](#)]
43. Zhou, Z.; Song, J.; Nie, L.; Chen, X. Reactive Oxygen Species Generating Systems Meeting Challenges of Photodynamic Cancer Therapy. *Chem. Soc. Rev.* **2016**, *45*, 6597–662649. [[CrossRef](#)] [[PubMed](#)]
44. Chen, K.; He, P.; Wang, Z.; Tang, B.Z. A Feasible Strategy of Fabricating Type i Photosensitizer for Photodynamic Therapy in Cancer Cells and Pathogens. *ACS Nano* **2021**, *15*, 7735–7743. [[CrossRef](#)] [[PubMed](#)]
45. Mroz, P.; Pawlak, A.; Satti, M.; Lee, H.; Wharton, T.; Gali, H.; Sarna, T.; Hamblin, M.R. Functionalized Fullerenes Mediate Photodynamic Killing of Cancer Cells: Type I versus Type II Photochemical Mechanism. *Free Radic. Biol. Med.* **2007**, *43*, 711–719. [[CrossRef](#)]
46. Gradova, M.A.; Movchan, T.G.; Khudyaeva, I.S.; Chernyad'ev, A.Y.; Plotnikova, E.V.; Lobanov, A.V.; Belykh, D.V. Synthesis of the Novel Cationic Chlorin Derivatives with a Phytol Fragment on the Periphery of the Macrocycle and Their Aggregation State in Aqueous Surfactant Solutions. *Macroheterocycles* **2020**, *13*, 23–32. [[CrossRef](#)]
47. Gradova, M.A.; Gradov, O.V.; Lobanov, A.V.; Bychkova, A.V.; Nikolskaya, E.D.; Yabbarov, N.G.; Mollaeva, M.R.; Egorov, A.E.; Kostyukov, A.A.; Kuzmin, V.A.; et al. Characterization of a Novel Amphiphilic Cationic Chlorin Photosensitizer for Photodynamic Applications. *Int. J. Mol. Sci.* **2023**, *24*, 345. [[CrossRef](#)]
48. Huang, L.; Wang, M.; Huang, Y.Y.; El-Hussein, A.; Wolf, L.M.; Chiang, L.Y.; Hamblin, M.R. Progressive Cationic Functionalization of Chlorin Derivatives for Antimicrobial Photodynamic Inactivation and Related Vancomycin Conjugates. *Photochem. Photobiol. Sci.* **2018**, *17*, 638–651. [[CrossRef](#)]
49. Pylina, Y.I.; Khudyaeva, I.S.; Startseva, O.M.; Shadrin, D.M.; Shevchenko, O.G.; Velegzhaninov, I.O.; Kukushkina, N.V.; Berezin, D.B.; Belykh, D.V. Dark and Photoinduced Cytotoxicity of Cationic Chlorin E6 Derivatives with Different Numbers of Charged Groups. *Macroheterocycles* **2021**, *14*, 317–322. [[CrossRef](#)]
50. Kruijtzter, J.A.W.; Hofmeyer, L.J.F.; Heerma, W.; Versluis, C.; Liskamp, R.M.J. Solid-Phase Syntheses of Peptoids Using Fmoc-Protected N-Substituted Glycines: The Synthesis of (Retro)Peptoids of Leu-Enkephalin and Substance P. *Chem. A Eur. J.* **1998**, *4*, 1570–1580. [[CrossRef](#)]
51. Kordatos, K.; Da Ros, T.; Bosi, S.; Vázquez, E.; Bergamin, M.; Cusan, C.; Pellarini, F.; Tomberli, V.; Baiti, B.; Pantarotto, D.; et al. Novel Versatile Fullerene Synthons. *J. Org. Chem.* **2001**, *66*, 4915–4920. [[CrossRef](#)] [[PubMed](#)]
52. Ulfo, L.; Cantelli, A.; Petrosino, A.; Costantini, P.E.; Nigro, M.; Starinieri, F.; Turrini, E.; Zadran, S.K.; Zuccheri, G.; Saporetti, R.; et al. Orthogonal Nanoarchitectonics of M13 Phage for Receptor Targeted Anticancer Photodynamic Therapy. *Nanoscale* **2022**, *14*, 632–641. [[CrossRef](#)] [[PubMed](#)]

53. Cantelli, A.; Malferrari, M.; Soldà, A.; Simonetti, G.; Forni, S.; Toscanella, E.; Mattioli, E.J.; Zerbetto, F.; Zanelli, A.; Di Giosia, M.; et al. Human Serum Albumin–Oligothiophene Bioconjugate: A Phototheranostic Platform for Localized Killing of Cancer Cells by Precise Light Activation. *JACS Au* **2021**, *1*, 925–935. [[CrossRef](#)] [[PubMed](#)]
54. Bortot, B.; Apollonio, M.; Baj, G.; Andolfi, L.; Zupin, L.; Crovella, S.; Di Giosia, M.; Cantelli, A.; Saporetti, R.; Ulfo, L.; et al. Advanced Photodynamic Therapy with an Engineered M13 Phage Targeting EGFR: Mitochondrial Localization and Autophagy Induction in Ovarian Cancer Cell Lines. *Free Radic. Biol. Med.* **2022**, *179*, 242–251. [[CrossRef](#)]

Disclaimer/Publisher’s Note: The statements, opinions and data contained in all publications are solely those of the individual author(s) and contributor(s) and not of MDPI and/or the editor(s). MDPI and/or the editor(s) disclaim responsibility for any injury to people or property resulting from any ideas, methods, instructions or products referred to in the content.